Meteorol Atmos Phys 91, 223–235 (2006)
DOI 10.1007/s00703-004-0099-2

Meteorology and Atmospheric Physics
Printed in Austria

Department of Atmospheric Sciences, University of California, Los Angeles, CA, USA

Cirrus cloud horizontal and vertical inhomogeneity effects in a GCM

Yu Gu and **K. N. Liou**

With 14 Figures

Received April 19, 2004; revised July 15, 2004; accepted August 12, 2004
Published online: April 28, 2005

Summary

A set of the inhomogeneity factor for high-level clouds derived from the ISCCP D1 dataset averaged over a five-year period has been incorporated in the UCLA atmospheric GCM to investigate the effect of cirrus cloud inhomogeneity on climate simulation. The inclusion of this inhomogeneous factor improves the global mean planetary albedo by about 4% simulated from the model. It also produces changes in solar fluxes and OLRs associated with changes in cloud fields, revealing that the cloud inhomogeneity not only affects cloud albedo directly, but also modifies cloud and radiation fields. The corresponding difference in the geographic distribution of precipitation is as large as 7 mm day^{-1}. Using the climatology cloud inhomogeneity factor also produces a warmer troposphere related to changes in the cloudiness and the corresponding radiative heating, which, to some extent, corrects the cold bias in the UCLA AGCM. The region around 14 km, however, is cooler associated with increase in the reflected solar flux that leads to a warmer region above. An interactive parameterization for mean effective ice crystal size based on ice water content and temperature has also been developed and incorporated in the UCLA AGCM. The inclusion of the new parameterization produces substantial differences in the zonal mean temperature and the geographic distribution of precipitation, radiative fluxes, and cloud cover with respect to the control run. The vertical distribution of ice crystal size appears to be an important factor controlling the radiative heating rate and the consequence of circulation patterns, and hence must be included in the cloud-radiation parameterization in climate models to account for realistic cloud processes in the atmosphere.

1. Introduction

Satellite mapping of the optical depth in midlatitude and tropical regions has illustrated that cirrus clouds are frequently finite in nature and display substantial horizontal variabilities (Minnis et al, 1993; Ou et al, 1995). Vertical inhomogeneity of the ice crystal size distribution and ice water content (IWC) has also been demonstrated in the microphysics balloon sounding observations (Heymsfield and Miloshevich, 1993). Based on three-dimensional (3D) radiative transfer calculations, cloud inhomogeneity has been shown to play a significant role in the heating rate profile averaged over mesoscale grids and the result differs from that computed from the conventional plane-parallel (PP) approach (Gu and Liou, 2001). However, creating representations of cloud inhomogeneity in general circulation models (GCMs) for climate study is a difficult task since they generally have spatial scales greater than 100 km due primarily to computational limitations. Moreover, the relationship between the cloud optical properties (in term of optical depth) and radiative fluxes is nonlinear, leading to biases in the model-simulated flux field caused by the use of an average optical depth to represent cloud spatial inhomogeneity.

The cloud horizontal inhomogeneity effect on solar albedo has been examined by Cahalan et al (1994), Kogan et al (1995), and more recently by Cairns et al (2000). Using data obtained from observations, large eddy simulations, and Monte-Carlo radiative transfer calculations for stratocumulus and cumulus clouds, these authors found that cloud inhomogeneity leads to a considerably smaller solar albedo, as compared to the value computed from the PP radiative transfer model employing a mean liquid water content (LWC). This effect has been taken into account in climate models by reducing the optical depth, e.g., by a factor of 0.7, for all cloud types. Tiedtke (1996) and Rotstayn (1997) tested the assumption of a uniform adjustment in GCMs, and pointed out that extension of the uniform reduction factor to all modeled clouds appears unrealistic but might be taken as the lower limit of the adjustment. Rossow et al (2002) used the International Satellite Cloud Climatology Project (ISCCP) datasets to obtain a climatology of the mesoscale variability of cloud optical depth, emissivity, and temperature to test and refine the treatment of cloud-radiation interactions. However, these inhomogeneity parameters have not been tested in a GCM.

The present study focuses on the high-level cirrus clouds that play a pivotal role in the radiative budget of the Earth-atmosphere system through the reflection of solar radiation and the trapping of outgoing longwave radiation, and hence, significantly affect the atmospheric thermal structure and climate (Liou, 1986; 1992; Ackerman et al, 1988; Stephens et al, 1990). Most of the previous studies on cloud inhomogeneity have focused on quantifying the solar albedo bias for stratocumulus clouds, where a bias as high as 15% has been reported (Cahalan et al, 1994; Barker, 1996; Pincus et al, 1999). Attention has recently been given to high-level clouds. A bias in the outgoing longwave radiative energy budget, up to $-15\,\mathrm{W\,m^2}$, has been found due to the high-level ice cloud inhomogeneity (Fu et al, 2000; Pomroy and Illingworth, 2000). Carlin et al (2002) examined the high ice cloud inhomogeneity using optical depth dataset for the midlatitude, and reported a solar albedo bias of up to 25% over a low reflective surface at a high solar zenith angle, and a spherical solar albedo bias as high as 11%. The high cloud inhomogeneity effect on simulated climate, however, has not been examined.

Cloud vertical inhomogeneity have been mostly studied in terms of cloud vertical overlap (e.g., Geleyn and Hollingsworth, 1979; Liang and Wang, 1997; Stubenrauch et al, 1997; Chou et al, 1998; Gu and Liou, 2001). Computation of the radiative properties of cirrus clouds requires the information on ice crystal size distribution and a time-consuming computational light-scattering program. Thus, parameterizations (e.g., Fu and Liou, 1993) have been developed to determine the single-scattering properties in terms of IWC and mean effective ice crystal size. While IWC is generally predicted in GCMs, mean effective ice crystal size is normally prescribed. For example, a value of 75 μm has been used by Köhler (1999) and Ho et al (1998). The ice crystal size distribution, however, is a function of temperature (Heymsfield and Platt, 1984), and significantly interacts with the radiation field (Gu and Liou, 2000; Wu et al, 2000). Thus, it would be desirable to develop an interactive mean effective ice crystal size parameterization in connection with radiative transfer calculations in GCMs and climate models.

The objective of this study is to investigate the effect of cirrus cloud horizontal and vertical inhomogeneity on climate simulation. We use the UCLA atmospheric GCM (AGCM) described in Sect. 2 to perform several numerical experiments, whose design is also discussed. In Sect. 3, we investigate the effect of the cirrus cloud horizontal inhomogeneity on the simulated climate in terms of precipitation, temperature, radiation, and cloud patterns, while the sensitivity of the simulated climate to cirrus cloud vertical inhomogeneity is discussed in Sect. 4. Finally, a summary is given in Sect. 5.

2. Model description and experiment design

2.1 UCLA AGCM

The UCLA AGCM is a state-of-the-art grid point model of the global atmosphere extending from the Earth's surface to a height of 50 km. The most important features of the model have been described in Gu et al (2003). The model predicts the horizontal wind, potential temperature,

mixing ratios of water vapor, cloud liquid water and ice water, planetary boundary layer depth, surface pressure, land surface temperature, and snow depth over land. In this study, we used a low-resolution version, with horizontal resolution of 4° latitude by 5° longitude and 15 vertical layers from the Earth's surface to 1 hPa. The recently updated UCLA AGCM incorporates a more physically based radiation scheme that has the capability of studying a variety of climate problems, including the greenhouse gas and aerosol effects (Gu et al, 2003). This scheme combined the delta-four-stream (Liou et al, 1988) and the delta-two-and-four-stream methods (Fu et al, 1997) for solar and thermal infrared flux transfer, respectively. Both methods have been demonstrated to be computationally efficient and, at the same time, highly accurate in comparison to exact radiative transfer computations. The correlated *k*-distribution method for radiative transfer was used to account for gaseous absorption in multiple scattering atmospheres. The single-scattering properties for ice and water clouds were parameterized in terms of IWC/LWC and mean effective size/radius. In conjunction with the preceding radiative scheme, parameterizations for the fractional cloud cover and cloud vertical overlap have also been devised in the model. The cloud amount is empirically determined from the total cloud water mixing ratio. For radiation calculation purposes, the model clouds were vertically grouped in terms of low, middle, and high cloud types. Maximum overlap was first used for each cloud type, followed by random overlap among the three groups.

2.2 Parameterization of cloud horizontal inhomogeneity

The general approach to account for cloud spatial inhomogeneity is to adjust the optical depth by an empirical value less than 1. The adjustment coefficients must be related to LWC and IWC fields in the cloud and values of 0.5 to 0.85 have been employed. To investigate the sensitivity of the cloud inhomogeneity factor in the UCLA AGCM, Gu et al (2003) carried out a simulation in which the cloud inhomogeneity factor of 0.7 was replaced by 1. This modification reduces OLR by $4.6\,\mathrm{W\,m^{-2}}$, and simultaneously enhances the reflected solar radiation by about $12\,\mathrm{W\,m^{-2}}$. The inhomogeneity effect on solar radiation clearly exceeds that on IR radiation. The corresponding planetary albedo increases from 27.82% to 31.31%, an enhancement of about 10%, indicating that the cloud inhomogeneity has a significant impact on the simulation of planetary albedo. Examination was also made of the effects of changing the mean effective ice crystal size from 85 μm to 50 μm. A reduction in ice crystal size leads to a smaller OLR at TOA, but a larger planetary albedo. The effect of ice crystal size on solar and IR radiation in these experiments had the same magnitude.

To investigate the cloud inhomogeneity effect on climate modeling, we performed a number of model simulations. Each simulation is a 5-year run with the initial condition corresponding to October 1. For the control run (CTRL), a reduction factor of 0.7 to account for cloud inhomogeneity was introduced to adjust the optical depth on each grid point for all cloud types in the UCLA AGCM simulation. Also, an ice crystal size of 80 μm was prescribed uniformly for ice clouds. A second simulation, referred to as HORZ, was conducted by replacing the uniform value of 0.7 with the five-year mean values of the inhomogeneity factor χ for high-level clouds that have been derived from the ISCCP D1 dataset (Rossow et al, 2002). These values were calculated from: (a) the area-mean optical depth τ_{m} obtained from an area of about 280 km by 280 km based on individual satellite pixels, representing an area of about 5 km by 5 km sampled at intervals of about 30 km as follows:

$$\tau_{\mathrm{m}} = \frac{1}{N}\sum_{i=1}^{N}\tau_i, \tag{1}$$

and (b) the corresponding radiative mean optical thickness τ_{r} that represents a homogeneous cloud having the same albedo as the actual inhomogeneous cloud with τ_{m} in the form

$$\tau_{\mathrm{r}} = R^{-1}\left\{\frac{1}{N}\left[\sum_{i=1}^{N}R(\tau_i)\right]\right\}, \tag{2}$$

where R is a radiative transfer operator that determines the radiative flux from the optical thickness. The inhomogeneity factor χ is then determined by

$$\chi = 1 - \tau_{\mathrm{r}}/\tau_{\mathrm{m}}. \tag{3}$$

The effects of cloud inhomogeneity on radiative transfer can then be approximately accounted for by re-scaling the area-mean optical thickness as follows:

$$\tau_r = (1 - \chi)\tau_m, \tag{4}$$

where τ_m is the linear average of varying optical thickness over the area that is predicted from a GCM, and τ_r is the "radiative-average" value that would yield the correct cloud albedo (Cairns et al, 2000).

Figure 1a and b shows, respectively, the geographic distribution of the annual mean values of χ averaged over 1986–90 for high-level clouds and the differences between $1 - \chi$ and a uniform value of 0.7. The distribution of χ illustrates the pattern of the ITCZ feature, the subtropical jet regions, the generation portion of winter storm tracks, and the clouds over major mountains. The most homogeneous high-level clouds are found over the eastern edges of the oceans in the southern hemisphere, north Africa, and the middle east (Fig. 1a). It is also shown that the reduction factor 0.7 may be a good approximation for clouds along the equator. However, for the fairly homogeneous areas, use of 0.7 may overestimate the cloud inhomogeneity effect (Fig. 1b). The geographic patterns of χ are rather constant with season. For this reason, we adopted the annual mean χ values and interpolated to the UCLA AGCM model grid point. Low and middle clouds remain unchanged in this experiment.

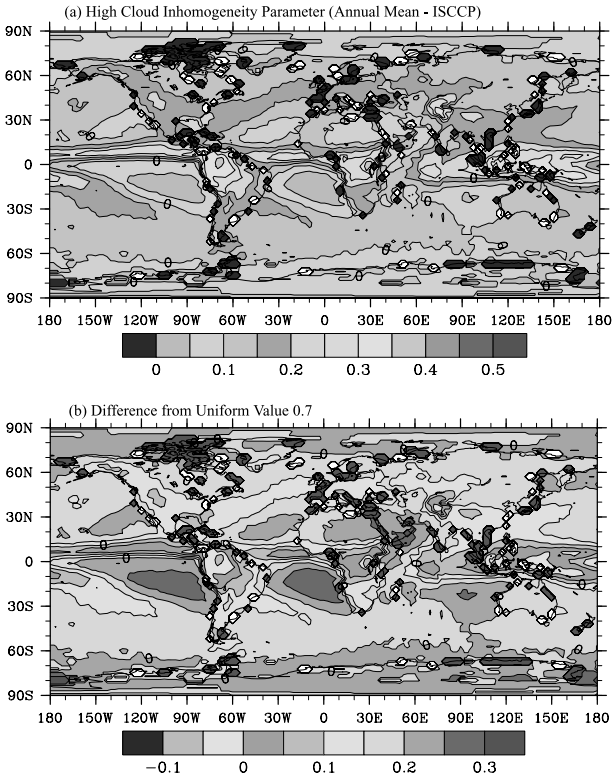

Fig. 1a. Geographic distribution of the annual mean values of the inhomogeneity factor χ averaged over 1986–90 for high-level clouds (ISCCP), (**b**) difference between $1 - \chi$ and a uniform value of 0.7 used in CTRL

2.3 Parameterization of ice crystal size for use in climate models

At this point, most of the climate models prescribe ice particle size in conjunction with radiation calculations. For example, the ice clouds in the UCLA AGCM assume a uniform ice crystal size of 85 μm (Gu et al, 2003). Using a two-dimensional cirrus cloud model with the explicit prediction of ice crystal size distribution, Gu and Liou (2000) showed that the lower parts of the cloud possess higher number densities of large ice particles, whereas the cloud top is dominated by the presence of more small ice particles. This result is consistent with the observed pattern presented by Heymsfield and Platt (1984), and Ou et al (1995), in which both IWC and mean ice crystal size show systematic relationship with temperature. Following the work of Liou (1992) and Ou et al (1995), the temperature-dependent IWC and mean effective ice crystal size may be expressed by parameterization in the forms

$$\overline{IWC} = \exp\{-7.6 + 4\exp[-0.2443\times10^{-3}(253 - T_c)]^{2.445}\}, \tag{5}$$

$$\overline{D_e} = \sum_{n=0}^{3} c_n (T_c - 273)^n, \tag{6}$$

where $213\,\mathrm{K} < T_c < 253\,\mathrm{K}$, $c_0 = 326.3$, $c_1 = 12.42$, $c_2 = 0.197$, and $c_3 = 0.0012$. The temperature-dependent $\overline{D_e}$ is obtained according to a general power relationship between ice crystal size distribution and IWC as reported by Heymsfield and Platt (1984) who showed that for a given temperature, values of the empirical coefficients are subject to uncertainty due to the observational data spread. Therefore, accuracy of the actual mean effective ice crystal size must be further

improved based on $\overline{D_e}$. Using the relationship between $\overline{D_e}$ and $\overline{IWC}$ and since the real D_e and IWC must have the same relationship based on dimensional analysis, we have

$$D_e = (IWC/\overline{IWC})^{1/3}\overline{D_e}. \quad (7)$$

This formulation has been verified by Ou et al (1995) using the balloonborne replicator data obtained during the First ISCCP Regional Experiment, Phase II, Cirrus Intensive Field Observation (FIRE-II IFO). To implement this parameterization in the UCLA AGCM, we first compute $\overline{IWC}$ and $\overline{D_e}$ from Eqs. (5) and (6), respectively. Then using the IWC predicted from AGCM, we can determine D_e following Eq. (7) for each grid point where ice cloud occurs. In this way, D_e can effectively interact with radiation as well as dynamic and thermodynamic fields in the climate model. The vertical inhomogeneity of cirrus clouds is then accounted for in the UCLA AGCM by using the varied mean effective ice crystal size calculated from model predicted IWC and temperature for high clouds, an experiment referred to as VERT.

3. Effect of cirrus cloud horizontal inhomogeneity

To illustrate the cloud inhomogeneity effects on radiation budget, we show in Table 1 the January and July global mean solar fluxes and OLRs at TOA and the surface for the three AGCM simulations described in Sect. 2. Compared to CTRL, HORZ enhances the reflected solar radiation by about $5\,\mathrm{W\,m^{-2}}$, and reduces OLR by $2\,\mathrm{W\,m^{-2}}$ (Table 1). The cloud inhomogeneity effect on solar radiation clearly exceeds its effect on thermal infrared radiation. The corresponding planetary albedo increases from 27.82% to 29.12%, showing an improvement of about 4%. Compared to the observed planetary albedo obtained from the Earth Radiation Budget Experiment, which has a value of 29.5% (±1%) for the global mean (Barkstrom and Smith, 1986), incorporation of a uniform reduction factor of 0.7 in the UCLA AGCM reduces the reflected solar fluxes at TOA by about 4%. Inclusion of a set of variable reduction values leads to an overall improvement of solar flux simulation.

Figure 2 shows the zonal mean differences in the January and July net solar and IR fluxes at TOA between HORZ and CTRL. The zonal mean differences in net solar fluxes at TOA between HORZ and CTRL occur mainly in the ITCZ and the storm track zones in the northern hemisphere winter, as well as near the pole of the northern hemisphere summer. Note that for solar fluxes, most of the changes occur in the summer hemispheres due to the seasonal change of the sun. Changes in the OLR are located in the ITCZ and oceanic midlatitudes. These features are directly associated with differences in the cloud inhomogeneity factor used in HORZ and CTRL. Carlin et al (2002) studied the relationship between solar albedo and high-cloud optical depth and found that there was normally a convex relationship between solar albedo and ice cloud optical depth, except under certain cases such as low optical depth for an overhead sun and a high reflective underlying surface where a concave relationship was found. A higher inhomogeneity factor of 0.7 was used in CTRL, a smaller cloud optical depth, which results in less reflected solar fluxes and more OLRs at TOA. Rossow et al (2002) obtained a similar conclusion based on global radiation calculations using the ISCCP data for one particular day in July, 1986.

However, this conclusion does not seem to be true when we examine the geographic radiative

Table 1. Global mean values of the January and July solar (SW) and infrared (LW) fluxes at TOA and the surface (SFC) for the three AGCM simulations

Variable	January global mean			July global mean		
	CTRL	HORZ	VERT	CTRL	HORZ	VERT
TOA SW ($\mathrm{W\,m^{-2}}$)	261.5	256.4	263.4	244.7	240.3	245.9
TOA LW ($\mathrm{W\,m^{-2}}$)	230.1	227.5	226.2	236.2	234.2	232.7
SFC SW ($\mathrm{W\,m^{-2}}$)	192.5	187.3	193.0	176.4	171.9	175.8
SFC LW ($\mathrm{W\,m^{-2}}$)	55.47	55.12	54.33	54.43	54.54	53.32

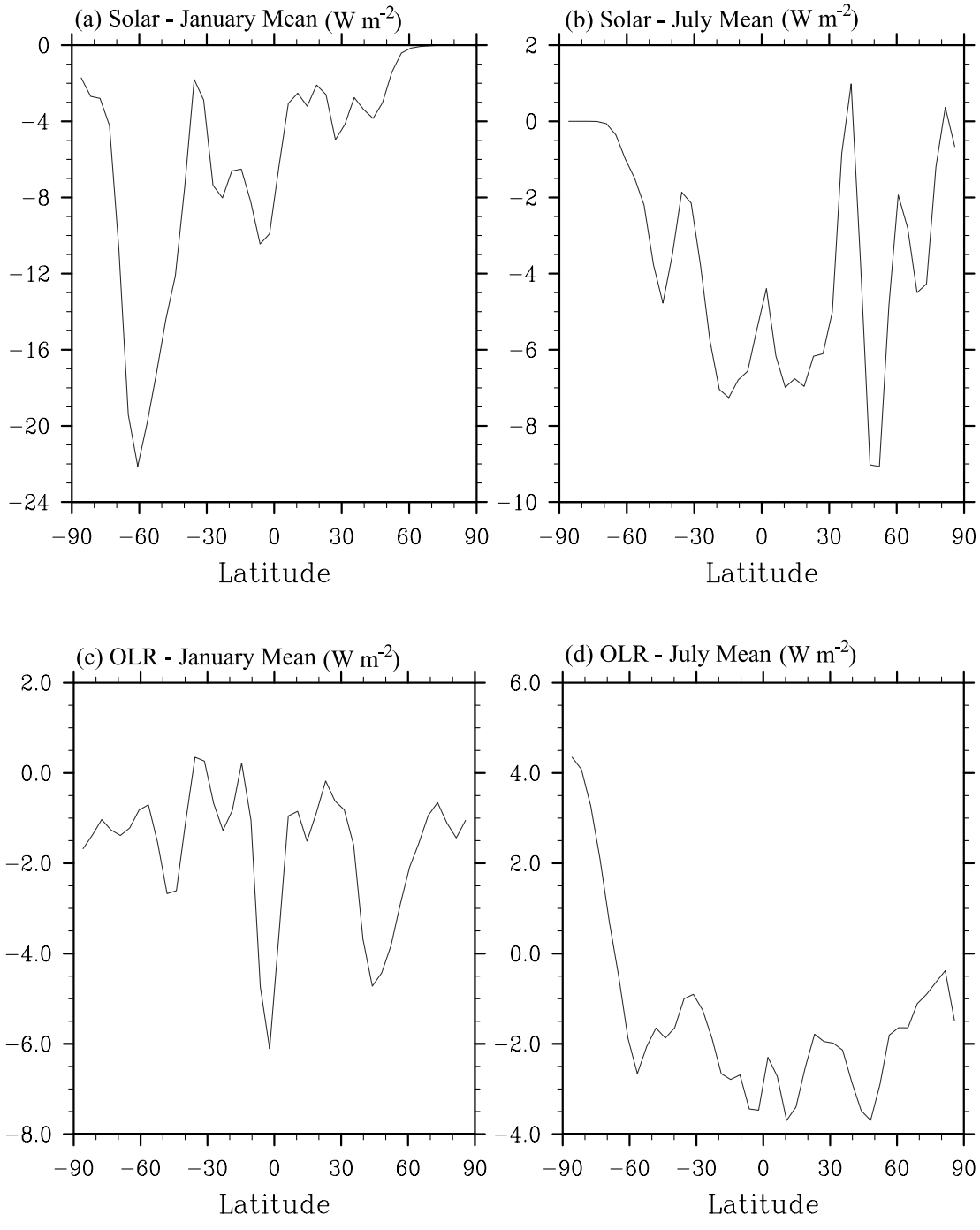

Fig. 2. Zonal mean differences in the January and July net shortwave (**a** and **b**), and longwave (**c** and **d**) fluxes (W/m^2) at TOA between HORZ and CTRL

flux distribution. Figures 3–5 display the distribution of the January and July mean solar and IR flux differences at TOA, and differences in the cloudiness. In January, differences in the solar flux are as large as $50\,W\,m^{-2}$, while more than $30\,W\,m^{-2}$ are found in OLRs (Figs. 3a and 4a). These differences do not display geographic patterns that resemble differences in the inhomogeneity field, as shown in Fig. 1b. Changes in the solar fluxes and OLRs, in fact, are associated with changes in the cloud fields (Fig. 5a). An increase (decrease) in cloudiness corresponds to a decrease (increase) in solar fluxes and OLRs. Comparing differences in the cloudiness with

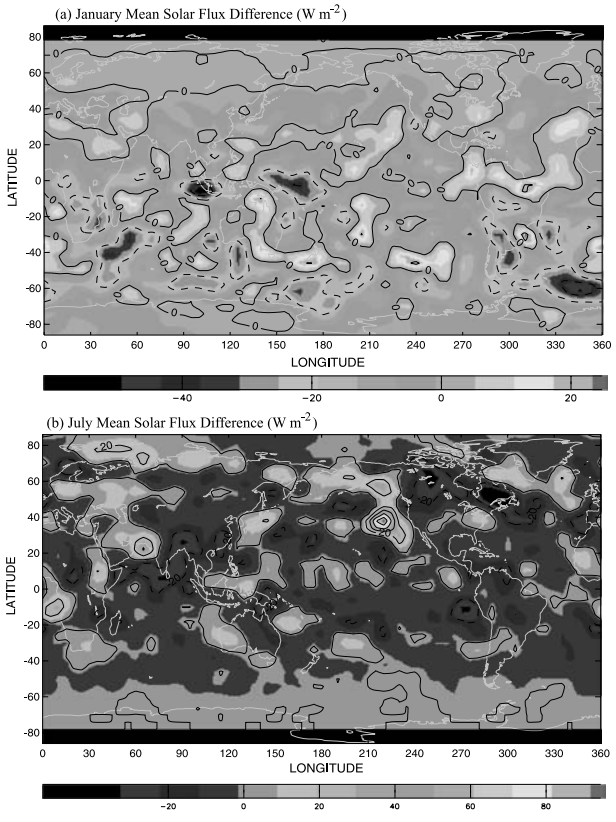

Fig. 3. January (**a**), and July (**b**) mean net solar flux differences (W m^{-2}) between HORZ and CTRL at TOA

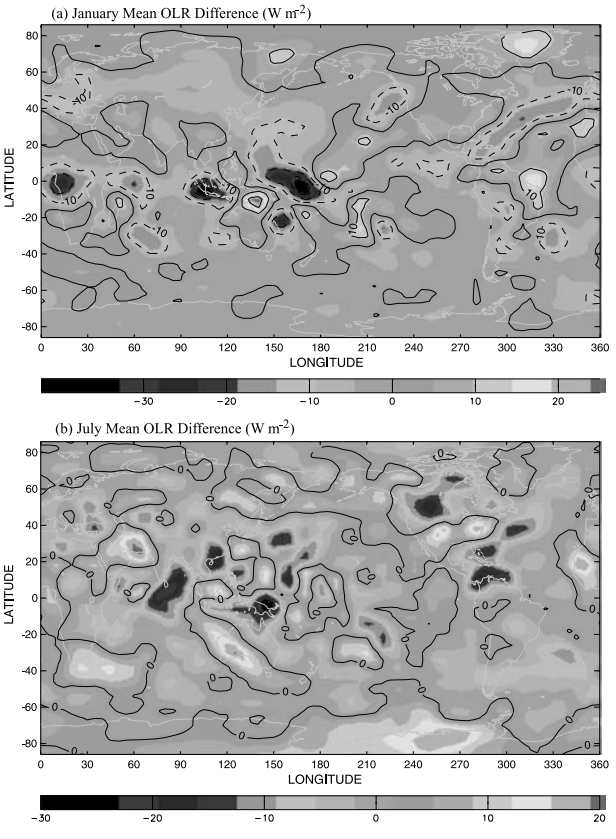

Fig. 4. Same as Fig. 3, except for OLR

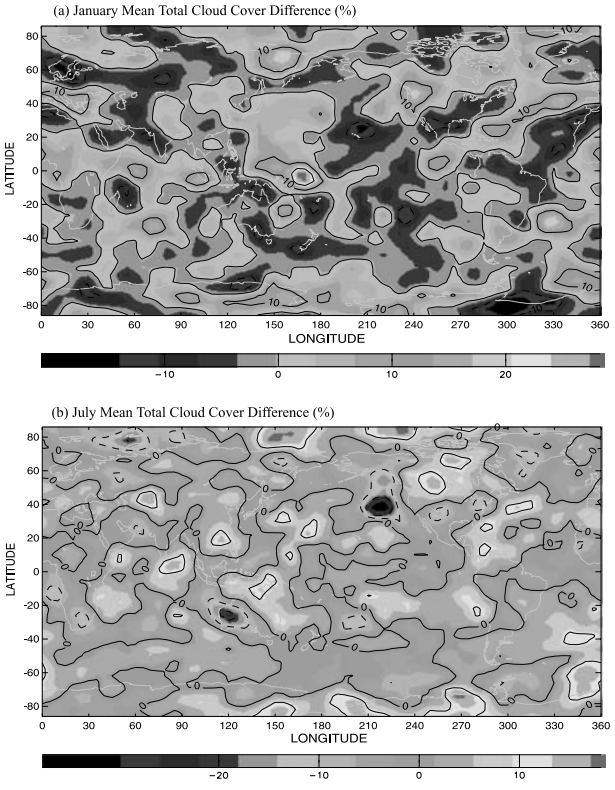

Fig. 5. January (**a**), and July (**b**) mean total cloud cover differences (%) between HORZ and CTRL

those in the inhomogeneity field (Fig. 1b), the increased cloudiness, hence more reflected solar flux, in some areas (e.g., along the equator from 0° E to the northeast of Australia) is associated with a higher inhomogeneity factor which, however, should give a smaller cloud albedo. This indirect feedback process could be due to the fact that initially the cloud with a higher inhomogeneity has a lower albedo and reflect less solar radiation. As a consequence, more heating occurs below the cloud top and stronger updraft is produced, leading to the formation of more cloudiness. Thus, cloud inhomogeneity not only affects the cloud albedo directly, but also modifies the global cloud field through cloud-radiation interaction. Similar changes are found in July in which radiative flux differences are also associated with changes in the cloudiness (Figs. 3b, 4b, 5b).

Figure 6 displays differences in the January and July mean precipitation distribution between the HORZ and CTRL experiments. Differences in the precipitation are found in ITCZ and the winter storm tracks with values as large as 7 mm day^{-1}, although the global mean values for the two cases are about the same. Differences in the geographic

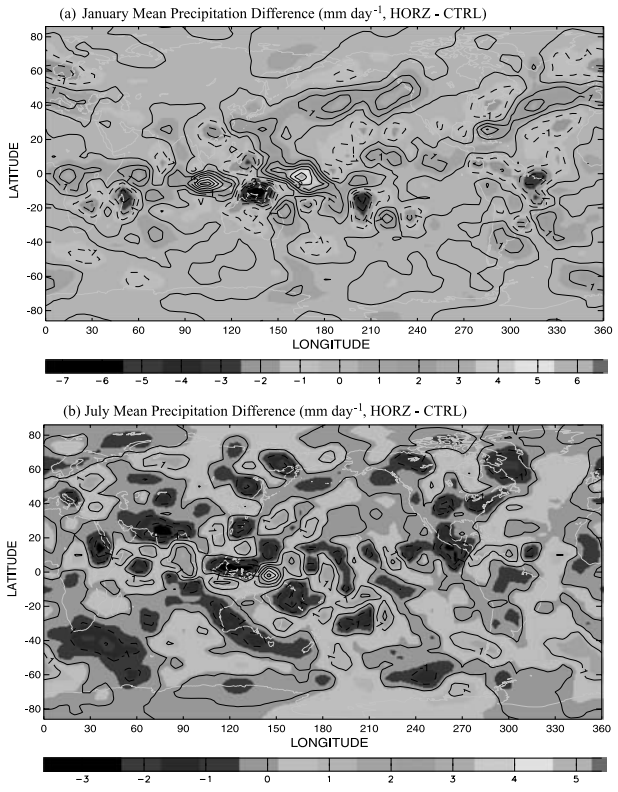

Fig. 6. January (**a**), and July (**b**) mean precipitation differences (mm day^{-1}) between HORZ and CTRL

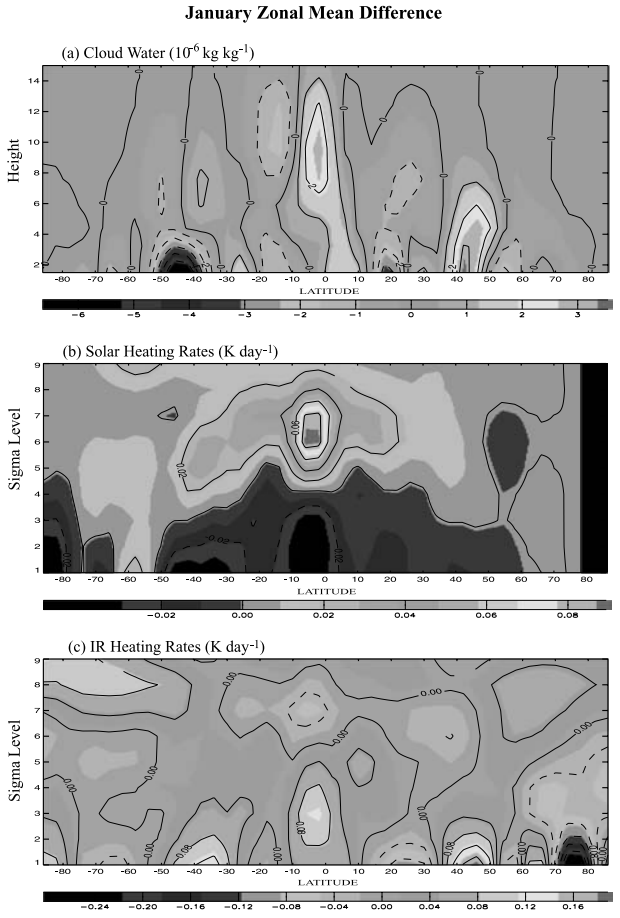

Fig. 7. January zonal mean differences in (**a**) the total cloud water mixing ratio (10^{-6} kg kg^{-1}), (**b**) shortwave heating rate (K day^{-1}), and (**c**) longwave heating rate (K day^{-1}) between HORZ and CTRL

distribution of precipitation, as in the case of radiative flux, do not display patterns that resemble those occurred in the inhomogeneity field. However, changes in the precipitation and radiative fluxes are closely associated with changes in the cloud fields (Fig. 5).

Figure 7 shows the January zonal mean differences in total cloud water mixing ratios, solar heating rates, and IR heating rates obtained in HORZ and CTRL. The HORZ experiment produces more cloud water in the middle to upper troposphere above the ITCZ and in the mid-lower troposphere of the midlatitudes in the northern hemisphere winter. Also HORZ produces more liquid water in the lower troposphere of the midlatitude in the summer hemisphere (Fig. 7a). Figure 7b and c show the corresponding differences in solar and IR radiative heating rates. More high clouds result in more solar heating in the cloud layer, whereas it is less in the layers below due to the reduced downward solar flux (Fig. 7b). Increase in high clouds also leads to more IR cooling at the cloud top and more IR warming at the cloud bottom. The heating/cooling effect produced by IR exceeds the solar heating, resulting in warming of the troposphere. The simulated results for July are similar to those for January and are not shown here.

The January and July zonal mean temperature differences between the HORZ and CTRL experiments are illustrated in Fig. 8. In January, HORZ produces a warmer surface and troposphere related to the net radiative warming in this region. This warming, to some extent, corrects the cold bias in the UCLA AGCM. However, the region around 14 km is cooler as a result of the variable cloud inhomogeneity that increases the reflected solar fluxes, as compared to the use of a uniform value of 0.7. Consequently, more upward reflected solar fluxes result in more absorption above and hence a warmer region, as shown in Fig. 8a. The July simulation results, however, differ somewhat with cooling in the troposphere of the oceanic midlatitudes due

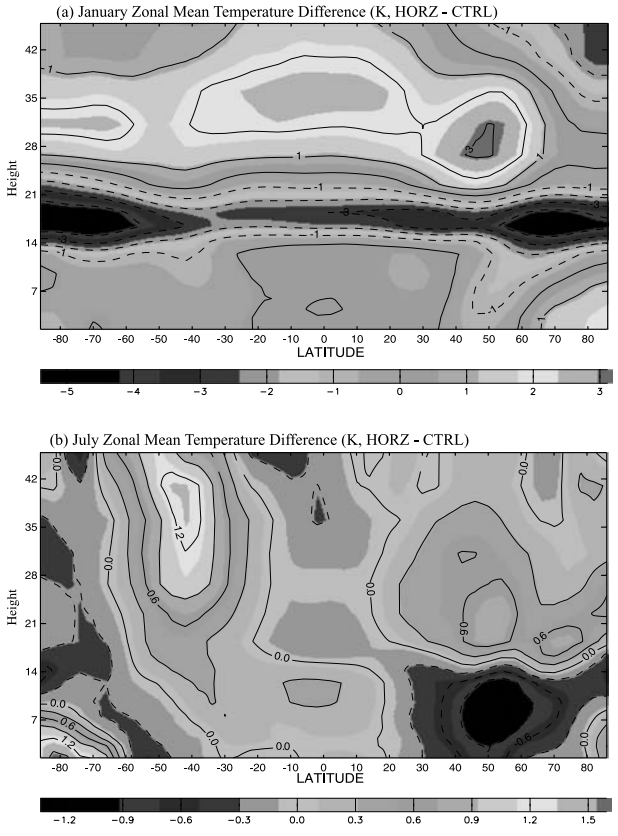

Fig. 8. January (**a**), and July (**b**) zonal mean temperature differences (K) between HORZ and CTRL

to less latent heat release in those areas associated with the reduced cloud field.

4. Effect of cirrus cloud vertical inhomogeneity

Using the formulation presented in Sect. 2.3, the relationship between the mean effective ice crystal size and IWC and temperature is displayed in Fig. 9. The D_e values for temperatures from $-60\,^{\circ}\mathrm{C}$ to $-20\,^{\circ}\mathrm{C}$ (213 to 253 K) and IWCs from 0.1 to $2\,\mathrm{mg\,m^{-3}}$ (left panel) and 2 to $40\,\mathrm{mg\,m^{-3}}$ (right panel) range between 15 and 150 µm, in general agreement with the mean effective ice crystal sizes retrieved from the FIRE-II IFO observation (Ou et al, 1995). These values are also in the size range determined from the 28 ice crystal size distributions obtained from six field campaigns reported by Fu (1996). The mean effective ice crystal size is shown to increase with IWC. However, its relationship with temperature appears more complicated. For temperatures from -55 to $-45\,^{\circ}\mathrm{C}$, D_e decreases with increasing temperature for a given IWC. Outside this temperature range, however, D_e increases with increasing temperature.

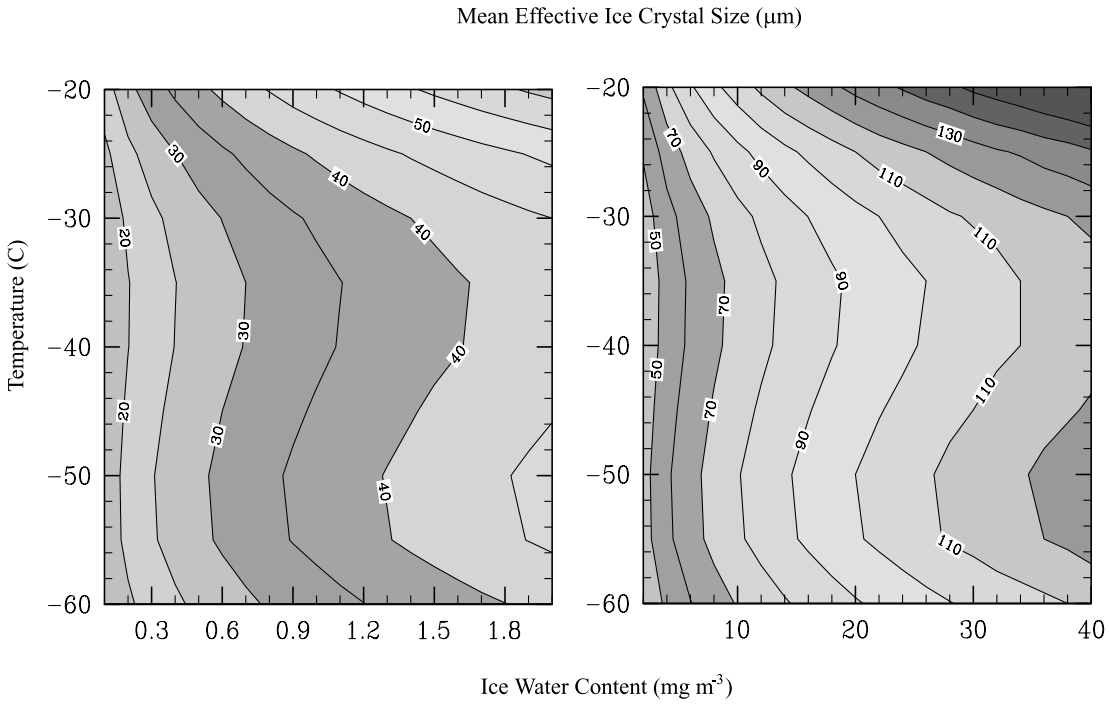

Fig. 9. Contour map of the mean effective ice crystal size (µm) as a function of ice water content (**a**) 0.1 to $2.0\,\mathrm{mg\,m^{-3}}$, and (**b**) 2.0 to $40\,\mathrm{mg\,m^{-3}}$ for temperature from -60 to $-20\,^{\circ}\mathrm{C}$

We now examine the cirrus cloud vertical inhomogeneity effect on the simulated climatic patterns in terms of mean effective ice crystal size. The January and July global mean radiative fluxes at TOA and the surface for VERT are listed in Table 1. At TOP, this experiment produces 1–2 $W\,m^{-2}$ differences in the global mean solar radiative flux and 3–4 $W\,m^{-2}$ in OLR, as compared to CTRL. It appears that the new interactive parameterization tends to generate an overall smaller mean effective ice crystal size (e.g., the January global mean value is about 58.18 μm) as compared to the prescribed 85 μm in CTRL. As a result, more IR radiation emitted from the surface is trapped in VERT than in CTRL. However, the global mean reflected solar flux decreases due to the reduced cloudiness. The mean effective ice crystal size appears to have more direct impact on IR radiation, while the cloudiness has larger impact on solar radiation.

The geographic distribution of the precipitation, OLR, and total cloud cover fields also shows substantial differences between VERT and CTRL. Increases in the precipitation over the winter storm track in January and over warm pool in both January and July are seen in VERT, with a maximum value of about 6 mm day^{-1} (Fig. 10). While CTRL underestimates the convection and precipitation in Indo-Pacific (Gu et al, 2003), VERT appears to improve the simulation in that area. The January and July global mean values of precipitation from VERT also show better agreement with observations (3.21 mm and 3.45 mm for January and July, respectively, according to the data reported in CMAP) than CTRL (Table 2).

The global mean cloud cover simulated from VERT is also slightly closer to the ISCCP observed value of 62.2% for January and 62.6% for July (Table 2). Difference in the cloud cover, with a maximum value of about 25%, has

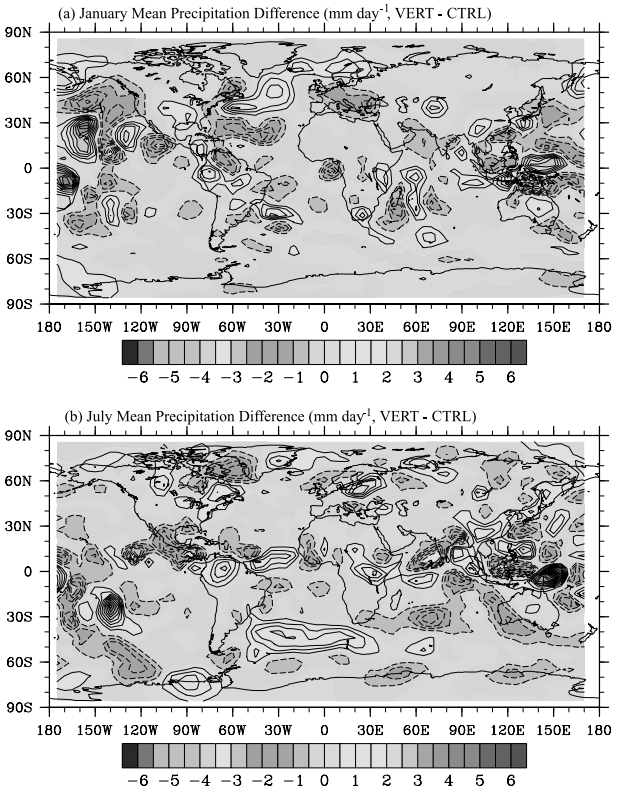

Fig. 10. January mean differences in (**a**) January, and (**b**) July precipitation (mm day^{-1}) between VERT and CTRL

a similar pattern as that in the precipitation, as is expected (Fig. 11). The corresponding difference in OLR is as large as 35 $W\,m^{-2}$ and has an opposite sign with respect to precipitation and cloud cover as a consequence of the thermal greenhouse effect of clouds (Fig 12). Negative values are found over warm pool, indicating the enhancement of the simulated convection in that region in VERT.

The January zonal mean ice water mixing ratio difference between VERT and CTRL shows more ice water in the high cloud regions over ITCZ and the subtropical oceanic area of the southern hemisphere (Fig. 14a). Consequently,

Table 2. Global mean values of total cloud cover, precipitation, and planetary albedo in the three AGCM simulations for January and July

Variables	January global means			July global means		
	CTRL	HORZ	VERT	CTRL	HORZ	VERT
Total cloud cover (%)	63.85	63.85	63.39	63.92	64.16	63.17
Precipitation (60° S–60° N; mm day^{-1})	3.61	3.58	3.51	3.798	3.776	3.71
Planetary albedo (%)	27.4	29.12	27.34	27.56	29.0	27.07

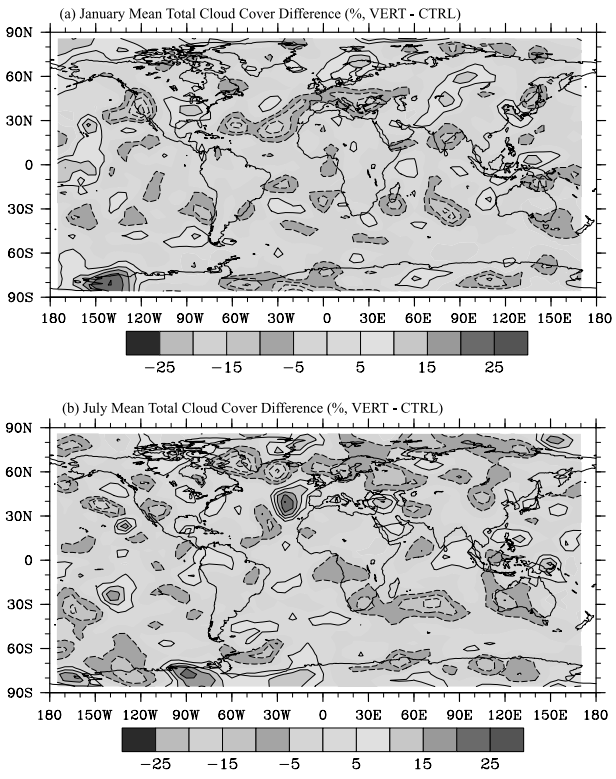

Fig. 11. January (**a**), and July (**b**) mean cloud cover differences (%) between VERT and CTRL

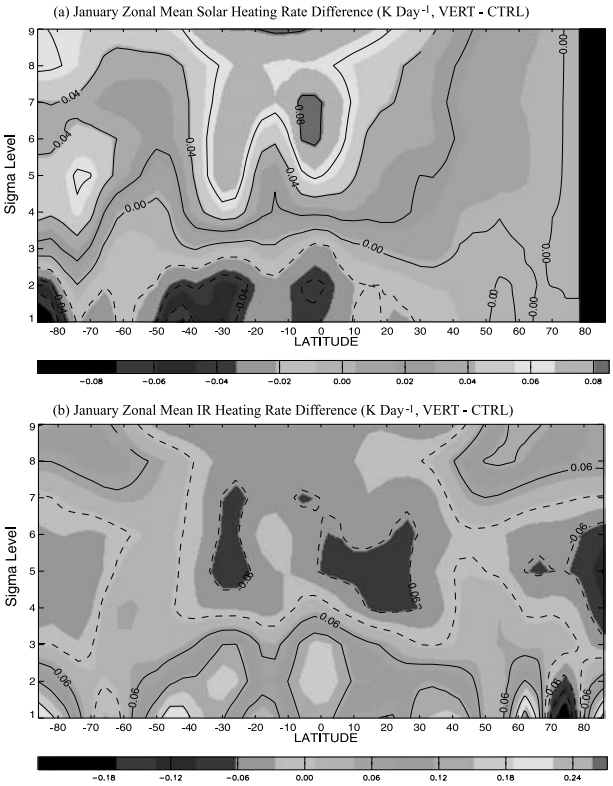

Fig. 13. January zonal mean (**a**) solar, and (**b**) IR heating rate differences ($\mathrm{K\,day^{-1}}$) between VERT and CTRL

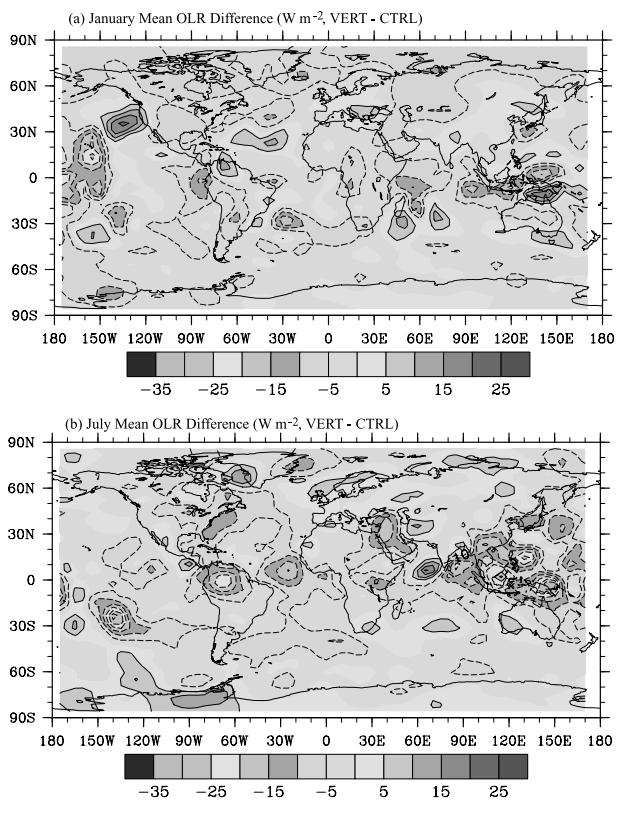

Fig. 12. January (**a**), and July (**b**) mean OLR differences ($\mathrm{W\,m^{-2}}$) between VERT and CTRL

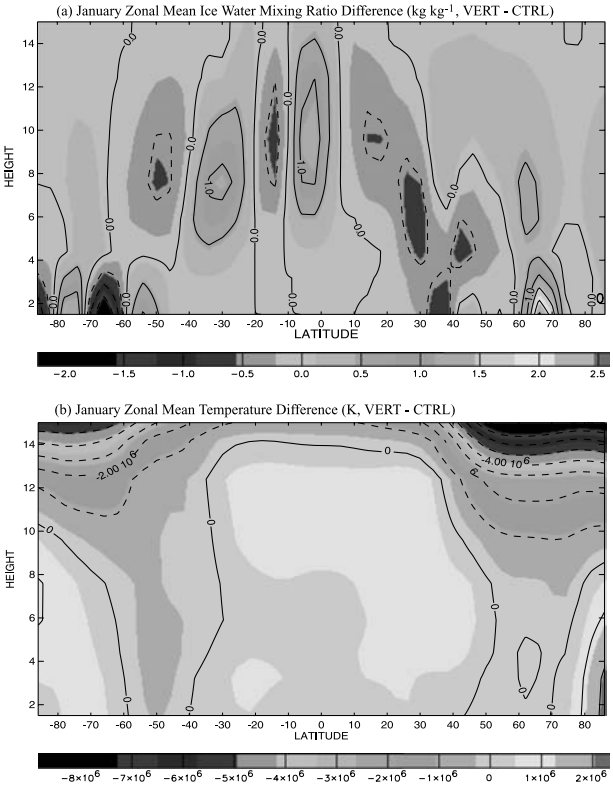

Fig. 14. January zonal mean (**a**) ice water mixing ratio ($\mathrm{kg\,kg^{-1}}$), and (**b**) temperature (K) differences between VERT and CTRL

more solar heating is found in VERT in those areas, while less is shown in the lower atmosphere due to decrease in the available solar flux (Fig. 13a). The IR heating rate shows enhanced cooling at the cloud top while more warming at the cloud bottom in accordance with changes in the ice cloud field (Fig. 13b). The corresponding zonal mean temperature differences illustrate warming in most areas of the troposphere associated with net radiative heating (Fig. 14b). Differences in July show similar patterns and are not presented here. It is clear that the new interactive parameterization for the mean effective ice crystal size is more physical and that the vertical inhomogeneity of cirrus clouds is an important factor that can significantly impact climate simulation.

5. Conclusions

The cirrus cloud horizontal and vertical inhomogeneity effects have been investigated in this study. The introduction of a cloud inhomogeneity factor with spatial variations leads to a significant increase in the net solar fluxes at TOA with a global average of about $5\,W\,m^{-2}$, compared to the use of a uniform value of 0.7. It improves the simulation of the reflected solar fluxes at TOA and hence the planetary albedo. The cloud inhomogeneity has an impact on the thermal radiative transfer as well, but the effect is quantitatively smaller. Differences in the precipitation distribution are as large as $7\,mm\,day^{-1}$, although the corresponding global mean value remains about the same. Differences in the geographic distribution of precipitation and radiative fluxes between the two different cloud inhomogeneity parameterizations are shown to be associated with the patterns of cloud field changes. An increase in the cloudiness in certain areas, and the consequent increase in the reflected solar flux and decrease in OLR, is associated with higher cloud inhomogeneity. Thus, cloud inhomogeneity not only affects cloud albedo directly, but also modifies the entire cloud and radiation fields. Using varied cloud inhomogeneity factors also produces temperature change in the whole atmosphere related to changes in the cloudiness and the corresponding radiative heating and latent heat release.

An interactive parameterization for mean effective ice crystal sizes based on IWC and temperature has been developed for use in climate models. The mean effective ice crystal size for a model grid when ice clouds are generated can now be parameterized from the predicted IWC and temperature in climate models. This allows a direct interaction between cloud microphysics and radiative transfer. The precipitation and cloud cover patterns simulated from the new parameterization show better agreement with the observed global mean values. The global mean effective ice crystal size calculated from the parameterization shows a smaller value than the prescribed 85 μm that was used in the control simulation, resulting in less OLR. In association with the reduced cloudiness, we also find that the reflected solar flux is smaller. The geographic distribution of the precipitation, OLR, and total cloud cover fields shows significant differences, as compared to the control run. More precipitation and less OLR are found in the winter storm track region and the Indian Ocean corresponding to changes in the cloudiness. Employing interactive mean effective ice crystal size results in a warmer troposphere associated with the radiative heating modulated by the cloudiness. The sensitivity of simulated climate to cloud horizontal (optical depth) and vertical (particle size) inhomogeneity appears to suggest that interactive parameterizations for these two parameters are required in order to improve the overall cloud and radiation physics currently used in climate models.

Acknowledgments

This research was supported by National Foundation Grant ATM-99-07924 and DOE Grant DE-FG03-00ER62904. We thank Drs. M. D. Chou and Xiaoqing Wu for constructive and useful comments on the paper.

References

Ackerman TP, Liou KN, Valero FP, Pfister L (1988) Heating rates in tropical anvils. J Atmos Sci 45: 1606–1623

Barker HW, Wielicki BA, Parker L (1996) A parameterization for computing grid-averaged solar fluxes for inhomogeneous marine boundary layer clouds. Part II: Validation using satellite data. J Atmos Sci 53: 2304–2316

Barkstrom BR, Smith GL (1986) The Earth Radiation Budget Experiment: Science and implementation. Rev Geophys 24: 379–390

Cahalan R, Ridgway W, Wiscombe W (1994) Independent pixel and Monte Carlo estimates of stratocumulus albedo. J Atmos Sci 51: 3776–3790

Cairns B, Lacis AA, Carlson BE (2000) Absorption within inhomogeneous clouds and its parameterization in general circulation models. J Atmos Sci 57: 700–714

Carlin B, Fu Q, Lohmann U, Mace G, Sassen K, Comstock JM (2002) High-cloud horizontal inhomogeneity and solar albedo bias. J Climate 15: 2321–2339

Chou MD, Suarez MJ, Ho CH, Yan MM-H, Lee K-T (1998) Parameterizations for cloud overlapping and shortwave single-scattering properties for use in general circulation and cloud ensemble models. J Climate 11: 202–214

Fu Q (1996) An accurate parameterization of the solar radiative properties of cirrus clouds for climate models. J Climate 9: 2058–2082

Fu Q, Liou KN (1993) Parameterization of the radiative properties of cirrus clouds. J Atmos Sci 50: 2008–2025

Fu Q, Liou KN, Cribb MC, Charlock TP, Grossman A (1997) Multiple scattering parameterization in thermal infrared radiative transfer. J Atmos Sci 54: 2799–2812

Fu Q, Carlin B, Mace G (2000) Cirrus horizontal inhomogeneity and OLR bias. Geophys Res Lett 27: 3341–3344

Geleyn J-F, Hollingsworth A (1979) An economical analytical method for the computation of the interaction between scattering and line absorption of radiation. Beitr Phys Atmos 52: 1–16

Gu Y, Liou KN (2000) Interactions of radiation, microphysics, and turbulence in the evolution of cirrus clouds. J Atmos Sci 57: 2463–2479

Gu Y, Liou KN (2001) Radiation parameterization for three-dimensional inhomogeneous cirrus clouds: Application to climate models. J Climate 14: 2443–2457

Gu Y, Farrara J, Liou KN, Mechoso CR (2003) Parameterization of cloud-radiation processes in the UCLA general circulation model. J Climate 16: 3357–3370

Heymsfield AJ, Miloshevich LM (1993) Overview of microphysics and state parameter measurements from FIRE-II. Proc. Conf. on FIRE Cirrus Science Results 1993, Breckenridge, CO, NASA, pp 1–4

Heymsfield AJ, Platt CMR (1984) A parameterization of the particle size spectrum of ice clouds in terms of the ambient temperature and ice water content. J Atmos Sci 41: 846–855

Ho C-H, Chou M-D, Surez M, Lau KM (1998) Effect of ice cloud on GCM climate simulations. Geophys Res Lett 25: 71–74

Kogan ZN, Lilly DK, Kogan YL, Filyushkin V (1995) Evaluation of radiation parameterizations using an explicit cloud microphysical model. Atmos Res 35: 157–172

Köhler M (1999) Explicit prediction of ice clouds in general circulation models. Ph.D. Diss., University of California, Los Angeles, 167 pp

Liang X-Z, Wang W-C (1997) Cloud overlap effects on general circulation model climate simulations. J Geophys Res 102: 11039–11047

Liou KN (1986) Influence of cirrus clouds on weather and climate processes: A global perspective. Mon Wea Rev 114: 1167–1198

Liou KN (1992) Radiation and cloud processes in the atmosphere. Oxford University Press, 487 pp

Liou KN, Fu Q, Ackerman TP (1988) A simple formulation of the delta-four-stream approximation for radiative transfer parameterizations. J Atmos Sci 45: 1940–1947

Minnis P, Liou KN, Takano Y (1993) Inference of cirrus cloud properties using satellite-observed visible and infrared radiances. Part I: Parameterization of radiance field. J Atmos Sci 50: 1279–1304

Ou SC, Liou KN, Coauthors (1995) Remote sounding of cirrus cloud optical depths and ice crystal sizes from AVHRR data: Verification using FIRE II IFO measurements. J Atmos Sci 52: 4143–4158

Pincus R, McFarlane SA, Klein SA (1999) Albedo bias and the horizontal variability of clouds in subtropical marine boundary layers: Observation from ships and satellites. J Geophys Res 104: 6183–6191

Pomroy HR, Illingworth AJ (2000) Ice cloud inhomogeneity: Quantifying bias in emissivity from radar observations. Geophys Res Lett 27: 2101–2104

Rossow WB, Delo C, Cairns B (2002) Implications of the observed mesoscale variations of clouds for the Earth's radiation budget. J Climate 15: 557–585

Rotstayn LD (1997) A physical based scheme for the treatment of stratiform clouds and precipitation in large-scale models. I: Description and evaluation of the microphysical processes. Quart J Roy Meteor Soc 123: 1227–1282

Stephens GL, Tsay S-C, Stackhouse PW, Flateau PJ (1990) The relevance of the microphysical and radiative properties of cirrus clouds to climate and climate feedback. J Atmos Sci 47: 1742–1753

Stubenrauch CJ, Del Genio AD, Rossow WB (1997) Implementation of subgrid cloud vertical structure inside a GCM and its effect on the radiation budget. J Climate 10: 273–287

Tiedtke M (1996) An extension of cloud-radiation parameterization in the ECMWF model. The representation of sub-grid-scale variations of optical depth. Mon Wea Rev 124: 745–750

Wu T, Cotton WR, Cheng WYY (2000) Radiative effects on the diffusional growth of ice particles in cirrus clouds. J Atmos Sci 57: 2892–2904

Corresponding author's address: Dr. Y. Gu, Department of Atmospheric Sciences, University of California, Los Angeles, CA 90095, USA (E-mail: gu@atmos.ucla.edu)